Journal of Neuroscience Methods 323 (2019) 82–89

Contents lists available at ScienceDirect

Journal of Neuroscience Methods

journal homepage: www.elsevier.com/locate/jneumeth

Invited review

Towards an efficient segmentation of small rodents brain: A short critical review

Riccardo Feo[a,b], Federico Giove[a,c,*]

[a] Centro Fermi–Museo Storico della Fisica e Centro Studi e Ricerche Enrico Fermi, 00184 Rome, Italy
[b] Sapienza Università di Roma, 00185 Rome, Italy
[c] Fondazione Santa Lucia IRCCS, 00179 Rome, Italy

ARTICLE INFO

Keywords:
Segmentation
Rat
Mouse
Brain

ABSTRACT

One of the most common tasks in small rodents MRI pipelines is the voxel-wise segmentation of the volume in multiple classes. While many segmentation schemes have been developed for the human brain, fewer are available for rodent MRI, often by adaptation from human neuroimaging. Common methods include atlas-based and clustering schemes. The former labels the target volume by registering one or more pre-labeled atlases using a deformable registration method, in which case the result depends on the quality of the reference volumes, the registration algorithm and the label fusion approach, if more than one atlas is employed. The latter is based on an expectation maximization procedure to maximize the variance between voxel categories, and is often combined with Markov Random Fields and the atlas based approach to include spatial information, priors, and improve the classification accuracy.

Our primary goal is to critically review the state of the art of rat and mouse segmentation of neuro MRI volumes and compare the available literature on popular, readily and freely available MRI toolsets, including SPM, FSL and ANTs, when applied to this task in the context of common pre-processing steps. Furthermore, we will briefly address the emerging Deep Learning methods for the segmentation of medical imaging, and the perspectives for applications to small rodents.

1. Introduction

A growing number of preclinical studies are based on mouse and rat MRI, both *ex vivo* and *in vivo*, thanks to the non-invasive nature of NMR and the availability of different contrasts and quantitative techniques. Common techniques involving small rodents include functional Magnetic Resonance Imaging (Jonckers et al., 2011, 2015), Diffusion Tensor Imaging (Zhang et al., 2012; Harsan et al., 2010), relaxometry (McIntosh et al., 2017; Soria et al., 2011), Voxel Based Morphometry (Ashburner and Friston, 2000; Sawiak et al., 2013) and Cortical Thickness studies (Tustison et al., 2013; Pagani et al., 2016; Nie et al., 2014).

A common step in MRI pipelines is the segmentation of the acquired volumes in different regions of interest or tissue classes. An expert human segmenter can effectively perform this step by labeling each MRI volume slice-by-slice, perhaps with the aid of an anatomical atlas, but this time consuming approach is often impractical. Indeed, the time required to perform it increases both with resolution and dataset size, while continuous development of MRI techniques and related increase of data quantity and quality worsen the problem. Furthermore, manual segmentations can display a large inter-rater variability, with volume overlaps usually varying between 80% and 95%, but depending on the specific regions, the overlap can be as low as 70% (Ali et al., 2005).

For over 30 years many algorithms have been developed to accelerate and standardize the process of MRI segmentation resulting in the variety of techniques that make up the current and still evolving state of the art. Most of these algorithms focused on human MRI, and it can be less than obvious which algorithms would better transfer to small rodents: while small rodent MRIs often offer lower contrast and less defined structures compared to human subjects, they also present less anatomical variability (Bai et al., 2012). Automated segmentation procedures can also be used to further enhance the registration algorithms themselves, as in the case of DARTEL from the popular SPM suite (Ashburner and Friston, 2005).

The purpose of this review is to present an overview of the state of the art of brain MRI segmentation for small rodents. After a brief introduction to common pre-processing steps, we will discuss atlas-based and statistical classification methods, and their implementation in some

* Corresponding author at: Dipartimento di Fisica, Sapienza Università di Roma, Piazzale Aldo Moro, 5, 00185 Roma, Italy.
E-mail address: federico.giove@uniroma1.it (F. Giove).

https://doi.org/10.1016/j.jneumeth.2019.05.003
Received 12 December 2018; Received in revised form 9 May 2019; Accepted 10 May 2019
Available online 15 May 2019

of the most used and freely available toolsets for brain MRI research.

Segmentation in itself is a complex procedure, including conceptually distinct steps. The main and historically oldest segmentation tasks in MRI literature is tissue classification (Zhang et al., 2001), which is aimed at a voxel-wise labeling of the MRI volume in a number of tissue classes, for example White Matter (WM), Gray Matter (GM) and Cerebrospinal Fluid (CSF), often achieved by employing expectation-maximization methods, Markov random fields and registration. Tissue classification is sometimes preceded by skull stripping, a specific segmentation task in which the brain parenchyma is separated from the rest of the MRI volume (mainly skull structures). While this can indeed be considered a special case of tissue classification, several ad-hoc methods have been developed for this task, which will be discussed separately.

Brain region segmentation instead attempts to identify within the MRI volume a set of regions of interest (ROIs) that have a distinct anatomical or functional meaning. In small rodents this is often based on registration alone, with the aid of one labeled atlas or by combining the labeling results from multiple atlases. In region segmentation pipelines a skull-stripping step is sometimes omitted, as the atlases employed may include a reference for the surrounding anatomy (Schwarz et al., 2006), and the skull-stripping procedures themselves can be registration-based (Leung et al., 2011). A straightforward implementation of a tool like FSL FIRST (Patenaude et al., 2011), combining manually labeled data and a Bayesian framework to segment several subcortical structures, is not currently available for rodents, although a similar procedure might be implementable with Atropos (ANTs) (Avants et al., 2011) in a more labor-intensive way. The segmentation methods presented in this review, unless stated otherwise, are all available for implementation in small rodents.

Strategies for rodents brain segmentation in MRI are still in active development. In addition to these approaches, we will also briefly discuss recent developments in the landscape of segmentation algorithms that are likely to be implemented for small rodents MRI in the near future. While artificial neural networks are not new in the field of MRI (Clarke et al., 1993; Schellenberg et al., 1990) the introduction of contemporary Deep Learning methods (LeCun et al., 2015; Ronneberger et al., 2015 Ronneberger et al., 2015) is likely to be one of the most important factors in the development of segmentation algorithms in the coming years.

2. Evaluation

In the available literature, the most common metrics to evaluate the results of segmentation and skull stripping algorithms are the Jaccard index J (Jaccard, 1912) and the Sørensen-Dice coefficient or Dice score D (Dice, 1945), defined as follows:

$$D = \frac{2\,|X \cap Y|}{|X| + |Y|}; \quad J = \frac{|X \cap Y|}{|X \cup Y|}$$

The two metrics can be used to quantify the similarity between two different segmentation masks, with a dimensionless index varying between 0 (no overlap) and 1 (perfect overlap). Both metrics contain the same information, and it is possible to calculate one from the other:

$$J = \frac{D}{2 - D}; \quad D = \frac{2J}{1 + J}$$

To evaluate the quality of a segmentation map a manual segmentation generally provides the ground truth, and the similarity between that and the algorithm's output provides a metric for the quality of the algorithm.

As popular as this metric is, it is not obvious that the average scores across many regions as measured by different studies can be compared directly. It is much easier to obtain high overlaps with large, bulky ROIs, while smaller and elongated regions are harder to successfully co-register. For this reason the most significant results when comparing different algorithms are the ones operating the same tasks, registering the same regions, on the same dataset.

3. Pre-processing

3.1. Intensity correction

The performance of both automated skull stripping and segmentation algorithms can be significantly enhanced by an intensity non-uniformity pre-processing step (Sled et al., 1998). The imperfections in the uniformity of the RF excitation field and receiver coil sensitivity profile often result in an artifact consisting in a smooth variation of the signal even in homogeneous tissues, called the bias field. While these effects in practice do not have a strong enough visual impact to impair manual segmentation, they can hamper the performance of automatic skull stripping and segmentation algorithms. Several algorithms have been developed to correct this bias, like the implementation of the procedure outlined by Sled et al. (1998) included in FreeSurfer, and it is recommended to implement a bias correction step before skull-stripping and segmenting the volumes.

3.2. Skull-stripping

Many analysis pipelines include a separate skull-stripping step, designed to discriminate brain and non-brain tissues. Several fully or semi-automated procedures have been developed for this purpose in the specific case of rodent MRI volumes (Table 1)

Pulse Coupled Neural Networks (PCNN) are a biomimetic neural network based on the visual cortex of cats (Zhan et al., 2017). In their original implementation PCNNs operated on individual 2D slices (Murugavel and Sullivan, 2009) but the algorithm has later been expanded to natively handle 3D data (Chou et al., 2011). 3D-PCNN remain competitive to this day, in some cases outperforming more recent methods like RATS (Oguz et al., 2014), in particular for skull-stripping in the presence of traumatic brain injuries (Roy et al., 2018). 3D-PCNN has been tested over the years on multiple datasets, with Dice scores generally above 0.9, up to 0.97 in ideal Signal-to-Noise Ratio conditions (Chou et al., 2011; Oguz et al., 2014; Roy et al., 2018; Li et al., 2013).

Table 1
Overview of automated skull-stripping programs.

Algorithm	Type	Comments
PCNN (Chou et al., 2011)	Neural network	Well established and effective
RATS (Oguz et al., 2014)	Graph segmentation	Developed to remain effective in low SNR T_1 volumes
rBET (Wood et al., 2013)	Based on BET	More recent and robust, reported slightly better performances compared to PCNN
3dSkullStrip-rat (Cox, 1996)		

The listed tools are freely available for research purposes at the following web addresses:
PCNN: https://sites.google.com/site/chuanglab/software/3d-pcnn.
RATS: https://www.iibi.uiowa.edu/rats-rodent-brain-mri.
rBET: https://www.nitrc.org/projects/rbet/.
3dSkullStrip: https://afni.nimh.nih.gov/.

Comparable scores have also been reported using methods based on constraint level sets (Uberti et al., 2009).

The RATS method, on the other hand, performs much better on T_1 volumes (Oguz et al., 2014), while most of the algorithms for rodent segmentation and brain extraction focus on T_2 volumes, as T_2 provides better contrast for small rodents.

While deformable surface methods developed specifically for human brain extraction can be inaccurate when applied directly to rodent MRI, they can be effectively adapted. In recent years Li et al. (2013), Wood et al. (2013) adapted the BET algorithm (Smith, 2002) to the rodent brain, both by improving on the algorithm itself and through a more appropriate choice of the shape prior. Both this implementation and the AFNI `3dskullstrip -rat` (Cox, 1996) function perform quite effectively, with Dice scores slightly above the 3D-PCNN method (Li et al., 2013; Roy et al., 2018).

Recently, Roy et al. (2018) applied Deep Neural Networks (LeCun et al., 2015) to the skull-stripping of both human and mice subjects with remarkable results, highlighting the robustness of these algorithms in the presence of traumatic brain injuries, with Dice scores around 0.95.

Semi-automated methods for skull-stripping are less time-efficient, but they can yield improved results. A common procedure, as outlined by Delora et al. (2016) and Pagani et al. (2016), is based on registering all mouse brains to study-specific template, to be segmented manually, and later propagate the brain mask to the individual volumes. While not fully automated this method yields excellent results, benefiting from being tailored to the specific experimental parameters of the study and the specific population, resulting in a reported Dice score of 0.96. In general, methods based on registration and single or multi-atlas segmentation are also common, implementing the same strategies that will be discussed for the segmentation of the rodent brain in a larger number of regions (Leung et al., 2011).

4. Segmentation

The task of brain region segmentation aims to identify a set of predefined regions in the rodent's brain, and relies on two key components to classify the different regions: a registration algorithm and one or more atlases, with the overall quality of the segmentation depending on both. The atlas or atlases contain the prior information on the tissue classes, in the form of labeled MRI volumes or templates, while the registration algorithm adapts the atlases to the volume to be segmented. The final output of the procedure is a new volume in which the labels and the original data to be segmented are co-registered in the same space.

In this section we will discuss in turn these key aspects of brain region segmentation and their implementation. Further on we will turn our attention to clustering algorithms and the different task of tissue segmentation. An overview of the general outline of a segmentation pipelines is given by the diagram in Fig. 1.

4.1. Single atlas segmentation

4.1.1. Atlases

The prior knowledge required to semantically segment different brain structures is often encoded in one or more anatomic atlases, composed of two volumes: the original MR data, or a template volume, and an associated voxel-by-voxel set of labels. Single MRI volumes, or a study-specific template, can be co-registered with the atlas or atlases to obtain a voxel-wise labeling of the volumes. Several atlases also feature probabilistic maps, where the probability of belonging to a particular class is mapped into each voxel, which can be seen as an early form of multi-atlas segmentation. Over the years, many atlases have been developed both for rats (including (Kjonigsen et al., 2015; Schweinhardt et al., 2003; Papp et al., 2014; Valdes Hernandez et al., 2011; Veraart et al., 2011; Rumple et al., 2013; Johnson et al., 2012; Schwarz et al., 2006; Hjornevik et al., 2007; Liang et al., 2017)) and mouses (including (Hjornevik et al., 2007; Dorr et al., 2008; Ma et al., 2005; Aggarwal et al., 2009; Johnson et al., 2010; Kovačević et al., 2004; Chuang et al., 2011)). Atlases can differ in many ways: template building strategy, contrasts, resolution, number of subjects, breed and age of the subjects, the use of *ex vivo* or *in vivo* data, coordinate reference, and segmentation classes.

A simple template building strategy is to choose one random subject and use a deformable registration algorithm to register this volume to every other brain, compute the inverse transforms and average them, to obtain a first average image. This process is then reiterated several times using the average as the new registration target (Kovačević et al., 2004). Using a template generated from multiple subjects allows avoiding errors due to imaging artifacts and individual variability, which might also be a consequence of excision in *ex vivo* brains. An alternative method is creating a minimum deformation template, building the average brain that minimizes the required deformation to be adapted to the entire database of individual subjects (Veraart et al., 2011; Johnson et al., 2012; Kochunov et al., 2001; Ma et al., 2005). Segmentations based on these templates can easily yield Dice scores above 0.9, with the exception of small or elongated structures, which are more sensible to slight registration errors (Ma et al., 2005). An effective template building strategy, based on the production of an initial reference through affine transformations and its refinement with a minimum nonlinear deformation approach, can be streamlined with the use of the `buildtemplateparallel` script available in the ANTs toolset (Avants et al., 2010).

A probabilistic atlas does not emerge from a direct segmentation of the template. Every volume used to build the template is manually segmented, and its final segmentation emerges from the statistics of the labels as they are propagated to the template.

Ex vivo atlases offer higher resolution and eliminate motion artifacts due to the breathing of the subject, however the brain itself is altered in the process. Aggarwal et al. (2009) observed a shrinkage in *ex vivo* brains from 1% up to (3.8 ± 0.6)% depending on the axis, and highlighted the problem of different structures shrinking by a different amount, also depending on the choice of reagents, concentrations and fixation methods. To address this problem an *ex vivo* template can be segmented and then non-linearly mapped to an *in vivo* population average (Aggarwal et al., 2009; Veraart et al., 2011).

The template itself can be segmented manually, or with the aid of an histological atlas. The popular Paxinos & Watson and Paxinos & Franklin atlases (Paxinos and Franklin, 2004; Paxinos and Watson, 1986), in their multiple versions, have been employed for this purpose by many authors, thus allowing for registration in stereotaxic coordinates.

Several attempts have been made at integrating the diverse landscape of available atlases and data for small rodents (Hawrylycz et al., 2011), including information such as function or gene and protein expression. The Waxholm space (Johnson et al., 2010), designed explicitly for MRI, CT and PET mouse brain imaging, is easy to convert to a stereotaxic reference, and is probably one of the most successful, but as of yet the general landscape of atlases remains quite varied.

4.1.2. Registration

Given one atlas, the atlas and the volumes to be segmented are registered to the same space. A common strategy in state of the art segmentation pipelines is to first build a study specific template, as discussed in the previous section for atlas building, and segment this template by co-registration with the atlas. The labels can then be propagated back to the individual subjects by inverting the transformations obtained (Pagani et al., 2016).

The quality of the labeling will be conditioned by the quality of the registration itself, and many strategies have been devised to improve this process. Image or volume registration is formulated as an optimization problem. Registration algorithms aim to find the optimal parameters for the transformation T, from the moving volume I_M to the

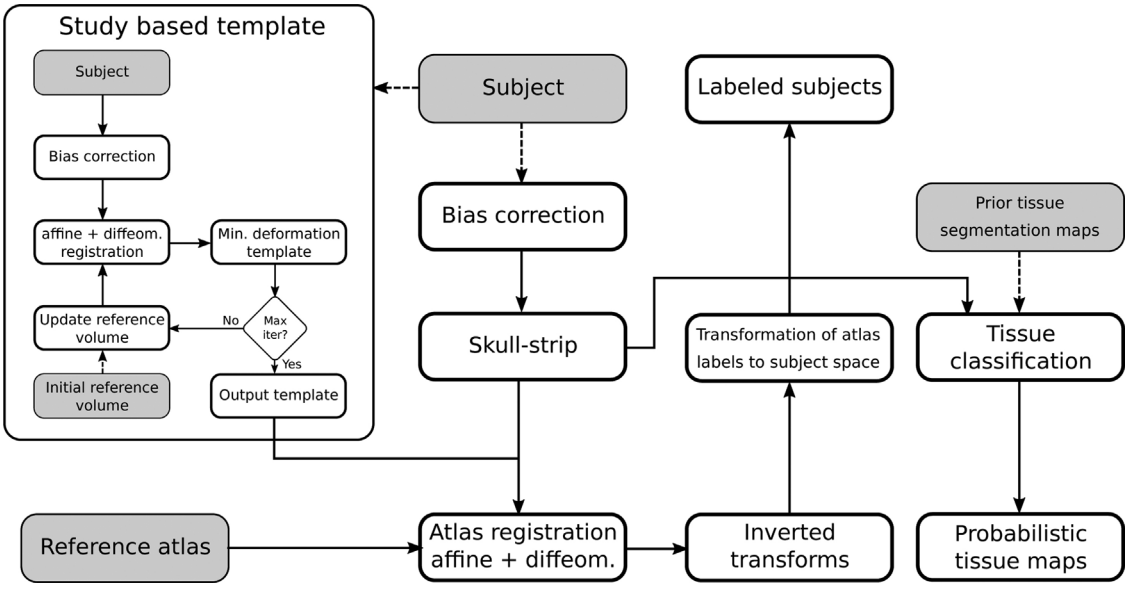

Fig. 1. General outline of segmentation pipelines including multiple tasks: skull stripping, region segmentation and tissue classification. Dashed lines indicate alternative or optional paths: for example, not all tissue classification algorithms require prior maps. This general outline can be modified and improved upon: for example one could implement a multi-atlas segmentation scheme, or a more complex template building strategy. Entire branches can be omitted, e.g. the user might be only interested in tissue classification. Depending on the toolset employed, some of these steps might be automated and transparent to the user.

target volume I_T, minimizing a cost function $C(I_M, I_T)$:

$$\hat{T} = \text{argmin}_{T \in S_T} C(I_M \circ T, I_T)$$

Where $I_M \circ T$ represents the I_M volume transformed by T, and S_T the space of allowed transformations T (consistently with the notation of Jenkinson and Smith (2001)). Linear transformations include translation, rigid registration, similarity, and affine, respectively allowing for translation only, then adding rotation, scaling, and shear. All of the most popular toolsets for MRI registration provide an easy way to implement these transformations out-of-the-box, including FLIRT from the FSL package (Jenkinson and Smith, 2001), ANTs (Avants et al., 2009), SPM12 (Penny et al., 2011), MNI_autoreg (Collins et al., 1994) and Elastix (Klein et al., 2010), and offer a variety of cost functions. Intra-modal registration is compatible with simple least squares or cross-correlation methods, while for inter-modal registration mutual information or normalized mutual information is often preferred. While these metrics are almost universally available, many toolsets feature cost functions that are not found in the others. A summary can be found in Table 2. While these tools have been primarily developed for humans, the algorithms used for linear registration do not require any particular fine tuning for the rodents. Many interpolation schemes are available after the algorithm has found the optimal transformation, however when transforming the atlas volumes a nearest neighbor interpolation is used to insure the labeling is preserved.

Table 2
Overview of the metrics available for linear registration algorithms in popular MRI research toolboxes.

AFNI	FSL	ANTs	MNI_AutoReg	Elastix
CR, Hellinger, LPC, MI, MS, NMI	CR, LD, MS, MI, NC, NMI	CC, CCH, GC, GD, ICP, JHCT, MS, MI, PSE	CC, MI, ND, SSC, VR	MS, MI, NC, NMI

Abbreviations: CC: cross correlation; CCH: histogram-based correlation coefficient; CR: correlation ratio; GC: global correlation; GD: gradient difference; ICP: iterative closest point (Euclidean); LPC: local Pearson correlation; JHCT: Jensen-Havrda-Charvet-Tsallis; LD: label difference; MS: mean squares; MI: mutual information; NMI: normalized mutual information; NC: normalized correlation; ND: normalized difference; PSE: point set expectation; SSC: cto-chastic sign change; VR: variance ratio. ICP, JHCT and PSE are designed for point-set registration.

State of the art registration and segmentation procedures implement affine transformations as a preliminary step, followed by non-linear, diffeomorphic mapping. A diffeomorphic transformation is a differentiable, non-linear transformation with a differentiable inverse, preserving the topological relationships of the subject's anatomy (connected or disjoint structures remain so) and ensuring that diffusion tensors remain positive definite, which is of primary importance in diffusion weighted imaging (Aggarwal et al., 2009). These large-deformations algorithms satisfy the inverse-consistency property, insuring that the matrices associated to the forward and reverse mappings are inverse to each other: invertibility is a key property of registration when applied to segmentation, to propagate the labels or probabilistic maps.

Bai et al. (2012) found that employing the Large Deformation Diffeomorphic Metric Mapping, LDDMM algorithm (Beg et al., 2005) for single atlas registration outperformed FFD and demons, with a mean dice score of 0.81 compared to 0.72 from affine registration, although at an high computational expense. Fu et al. (2017) compared one linear algorithm (FLIRT) and four diffeomorphic algorithms: DARTEL, geodesic shooting (optimizations of LDDMM, (Ashburner, 2007; Ashburner and Friston, 2011 Ashburner and Friston, 2011), diffeo-demons, geodesic-SyN and greedy-SyN (from ANTs). The best performing algorithms were geodesic-SyN and greedy-SyN (Avants et al., 2008, 2009), with mean volume overlaps of 0.77 and 0.76 respectively, the overlap of the affine registration averaging at 0.68 across all regions.

The demons algorithm searches for a diffeomorphic transformation with a diffusion based model (Thirion, 1998), whereas both LDDMM and SyN are based on the optimization of a velocity field mapping one volume to the other trough an integration step. While LDDMM is symmetric in theory, the optimization problem in not formulated symmetrically. By contrast, Avants et al. (2008) implemented an algorithm that exploits the inherent symmetry of the problem and guarantees that the path from the fixed to the moving volume remains the same when the roles are reversed, by defining an appropriate variational energy insuring that the two volumes contribute equally to the path. Geodesic-SyN allows for an unconstrained optimization within the space of diffeomorphic transformations, resulting in an higher accuracy compared to greedy-SyN. While the latter is an approximated

approach, it offers a major improvement in terms of speed, at the price of a very small loss in accuracy. For the same registration task, Fu et al. (2017) measured a running time of 103.2 min when performed with geodesic-SyN, and 27.8 min with greedy-SyN.

Klein et al. (2009) also highlighted the high accuracy of geodesic-SyN for brain MRI registration in human subjects, however direct application of SyN algorithms with human optimized parameters to rodent populations is not recommended. Fu et al. (2016) showed that optimizing the parameters of the SyN protocol for mices results in a 18% improvement of the Dice score compared to the SyN protocol optimized for humans, and a 22% improvement over affine registration. Applying SyN with human-optimized parameters only resulted in a minor improvement compared to the overlap achieved with linear registration methods. Fu et al. (2017) recommend large gradient descent steps, as the anatomical variability in mouses is lower than in humans, keeping the number of time points fixed at 2, and a time integration step of 0.05, employing a Gaussian regularizer with $\delta^2_{\text{gradient}} = 3$ and $\delta^2_{\text{total}} = 2$, and using cross correlation as a the similarity metric.

While according to Fu et al. (2017) they performed worse in high resolution MRI, the DARTEL and geodesic shooting algorithms for SPM12 are also widely used. Both tools are based on an intermediate tissue segmentation step based on a clustering method, registering simultaneously different tissue classes. To the authors knowledge the FNIRT tool included in FSL has not been compared to the ANTs or SPM12 tools in small rodents, but it does not appear to outperform them in humans (Klein et al., 2009).

Unlike AFNI's `3dQwarp` (Cox, 1996), which constructs a diffeomorphic transformation by a composition of diffeomorphisms, FNIRT builds one as a sum of diffeomorphic transformations. While this does not guarantee that the sum would be diffeomorphic, FNIRT approaches this problem by rejecting at each iteration non-diffeomorphic deformation fields and projecting them on the closest diffeomorphic field. This allows for the selection of transformations characterized by a Jacobian within a specified range, whereas different algorithms might result in diffeomorphic transformations with a Jacobian arbitrarily close to zero. The Jacobian determinant of a diffeomorphic transformation can itself be used to characterize local contractions or expansions, allowing for the localization of voxel-level differences in the local shape of brain structures (Pagani et al., 2016). FNIRT allows for the direct selection of the optimal deformation withing a specified range. A more comprehensive list of toolsets for nonlinear registration can be found in Tables 3 and 4.

4.2. Multi-atlas segmentation

One single atlas is often unable to characterize individual variability, and its propagation turns into systematic errors all random errors in the atlas building process. An effective alternative to single atlas segmentation is to employ a database of different atlases, computing the final segmentation using several manually segmented volumes. Each atlas is registered to the target volume, and the final segmentation is derived through a label fusion procedure. The general idea of multi-atlas segmentation resulted in a large variety of techniques for the labeling of biomedical images (Iglesias and Sabuncu, 2015) and it can be considered a class of supervised learning algorithms, several of which have been employed for the segmentation of rodent brain MRI.

Lancelot et al. (2014) demonstrated a marked improvement of a simple majority voting strategy over both single atlas and the propagation of one probabilistic atlas for the rat brain. Bai et al. (2012) compared several common registration and label fusion strategies for the segmentation of *in vivo* mouse brains. They investigated the interplay of affine, FFD, Demons and LDDMM registrations with majority voting, STAPLE and Markov Random Fields (MRF) as label fusion strategies, comparing them to single atlas segmentation. The quality of the registration step remained the most important variable, resulting in the highest Dice score improvements. LDDMM registration improved the average Dice score from 0.724 (affine registration) to 0.812 for single atlas registration, while multi-atlas methods improved the final overlap scores by about 0.03–0.04. The best results were obtained by combining LDDMM registration with either majority voting or STAPLE, resulting in a dice score of 0.845.

The MRF approach (Bae et al., 2009) jointly models the distribution of a voxel labels with its neighborhood, while the STAPLE algorithm (Warfield et al., 2004) estimates the performance of each generator atlas and constructs an estimate of the “true” segmentation via an expectation-maximization algorithm. Unlike a majority vote rule, which selects at each voxel the most frequent label, STAPLE is able to identify the correct segmentation even when there are repeated errors in a majority of the segmentations (Warfield et al., 2004). However the higher complexity of these algorithms, originally developed for human subjects, did not constitute a significant improvement over a much simpler majority voting strategy for the mouse brain, presenting subtler anatomical variations Bai et al. (2012).

STEPS (Cardoso et al., 2012, 2013) incorporates a local similarity metric in the STAPLE algorithm and combines it with a MRF model to address the problem of global vs. local image matching. Ma et al. (2012, 2014) confronted it with STAPLE and single-atlas registration after optimizing the parameters required by STEPS with a grid search, highlighting a marked improvement over both procedures on their dataset. The overall Dice score improvement granted by multi-atlas methods is not equally distributed among brain regions. Harder to segment brain structures like the fimbria and the anterior commissure register the highest improvements, of about 0.2 (Ma et al., 2012, 2014; Bai et al., 2012), while improvements in the thalamus or the cerebellum were smaller by one order of magnitude. The STEPS algorithm is distributed by the authors as part of NiftySeg.

Nie and Shen (2013) proposed a weighed average approach in which the quality of the local alignment is estimated with a mutual information strategy combined with a demons registration approach, implementing a support vector machine classifier. They report an

Table 3
Overview of the metrics available for nonlinear registration algorithms in popular MRI research toolboxes.

Toolbox	Metrics	Nonlinear transformations options
ANTs	CC, Demons, GC, ICP, MS, JHCT, Mattes, MI, PSE	BSplineDisplacementField, BSplineExponential, BSplineSyN, Exponential, GaussianDisplacementField, SyN, TimeVaryingBSplineVelocityField, TimeVaryingVelocityField
AFNI	CP, Hellinger, LPC MI, NMI, P	Piecewise polynomial C1 diffeomorphism
FSL	MS	FNIRT
Elastix	MS, MI, NC, NMI	B-splines, Thin-plate splines, SplineKernelTransform, WeightedCombinationTransform, BSplineTransformWithDiffusion, BSplineStackTransform
SPM12	Multinomial model	Geodesic shooting, DARTEL

Abbreviations: CC: cross correlation; CCH: histogram-based correlation coefficient; CP: clipped Pearson; CR: correlation ratio; GC: global correlation; GD: gradient difference; ICP: iterative closest point (Euclidean); JHCT: Jensen-Havrda-Charvet-Tsallis; LD: label difference; LPC: local Pearson correlation; MS: mean squares; MI: mutual information; NMI: normalized mutual information; NC: normalized correlation; ND: normalized difference; P: Pearson Correlation; PSE: point set expectation; SSC: stochastic sign change; VR: variance ratio. ICP, JHCT and PSE are designed for point-set registration.

Table 4
Overview of diffeomorphic registration approaches.

Algorithm	Type	Comments
Demons	Surface deformation	Often preferred for some application outside the scope of this work, e.g. feature extraction
SyN, Splines	Deformation field	Available in several variants, providing state of the art results in terms of accuracy
DARTEL	Combined with a clustering step	Popular tool in SPM, requires a prior tissue segmentation map, reported to be less effective in high resolution MRI (Fu et al., 2017)
FNIRT	Sum of deformation fields	User can specify the range of allowed local deformations

improved 0.859 Dice score over the initial 0.788 single-atlas overlap for *in vivo* volumes, and respectively 0.90 and 0.85 scores for in vitro volumes. Lee et al. (2014) also implemented a majority voting strategy weighed by intensity similarity after a b-spline deformation driven by corresponding particles, reporting a 0.05 overlap improvement over the 0.84 score for the pairwise registration.

While all of these authors provided Dice scores to evaluate their results, direct comparison of Dice scores across different studies, focusing on different atlases and different ROIs, is not necessarily meaningful. We can note however that it approaches the inter-rater overlap between different human raters (Ali et al., 2005).

4.3. Clustering methods

A different approach to tissue segmentation is to frame it as a clustering problem, labeling the individual voxels as members of different tissue classes. One of the classical tasks this algorithm is applied to is a 3 classes segmentation of gray matter, white matter and cerebrospinal fluid. MRI volumes provide effective contrast between these classes, but the problem is complicated by the bias field, noise and partial volume effects.

Earlier statistical approaches attempted to label single voxels based on probability values determined from the intensity distribution of the image, treating voxels as independent samples drawn from a population. Zhang et al. (2001) combined an expectation maximization approach with a Markov Random Field model (Li, 1994; Tohka et al., 2010) to take into account the spatial context of the specific voxels, articulated in a three steps expectation maximization algorithm alternating estimates of the class labels, distribution parameters and bias field, to maximize the interclass variance. This algorithm is currently implemented as the FAST tool in the FSL toolbox. As the initial estimates can suffer in the presence of strong bias fields the algorithm can also be initialized with an *a priori* probability map. The number of classes can also be increased, for example to account for strong lesions, or reduced, if the WM-GM contrast is too small in the target volume.

Ashburner and Friston (2005) developed the algorithm that would be implemented in SPM, combining registration and Gaussian mixture clustering. While this expectation maximization algorithm does not explicitly model spatial dependency in the same way of a MRF, context information is derived from the deformable registration of a probabilistic map of the different tissue classes. At each step the mixture parameters, bias fields and deformation are estimated separately while keeping the others constant. As of the current implementation in SPM12, the algorithm supports segmentation in several classes: GM, WM, CSF, bone, soft tissue, background/air. Each class is described by multiple Gaussians to account for partial volume effects and for the possibility that the true distribution might not be normal. Sawiak et al. (2009) developed a toolbox to facilitate the extension of SPM functionality to the animal brain, including mouse specific priors out-of-the-box, called SPMMouse.

The Atropos tool (Avants et al., 2011) included in ANTs implements an n-tissue segmentation algorithm capable of integrating multimodal information to enhance the segmentation performance with minimal memory requirements. Combining both of the strategies described above Atropos can include either MRFs, template based priors or a weighted combinations of both, as well as bias correction. It can also be used for brain extraction and label propagation from a probabilistic atlas. Atropos supports partial volume classes, for example the class of voxels containing both WM and GM can be classified as a separate category.

Supporting different initialization and optimization strategies, likelihood models, and optimization options, Atropos is a powerful tool with a significant number of parameters the user can tweak to fine tune the tool to their specific needs, and it has been applied to very different tasks like the segmentation of cysts in mouse kidneys tissues (Xie et al., 2015). However this is not always a benefit, and in some cases a more straightforward approach like the ones previously described can still yield good results with less fine-tuning. Table 5 presents a short summary of the methods here discussed.

In the case of *ex vivo* studies, the fixation procedure can severely impact the performance of a classic 3-classes segmentation. Pagani et al. (2016) and Li et al. (2009) worked around the overestimation of WM tissue at the expense of GM with Atropos and FSL respectively when implementing voxel based morphometry measures, by increasing the number of classes and reconstructing GM by merging the new classes appropriately. However the large loss of CSF as a consequence of fixation still impaired the quality of WM/CSF discrimination (Pagani et al., 2016).

5. Future perspectives

Many of the methods discussed here reach overlap scores comparable to those obtained between segmentations from different human raters (Ali et al., 2005). Beyond posing a ground truth problem, which can still be defined as a multi-atlas labeling of the same volume obtained from multiple human experts, these results are obtained at a steep cost in terms of computational resources, and become impractical when applied to large datasets. For this reason one of the biggest challenges in current classification tasks is computational efficiency.

An emerging approach, to the authors knowledge not yet implemented in small animals, is predictive registration (Gutierrez-Becker et al., 2017; Dalca et al., 2018; Yang et al., 2017). A machine learning

Table 5
Clustering based tissue classification tools included in the SPM12, FSL and ANTs toolboxes. Atropos also represents a valid choice for multi-atlas label fusion.

Algorithm	Toolbox	Comments
Unified segmentation	SPM12	Popular algorithm requiring spatial priors, MATLAB integration
FAST	FSL	Can include but does not require priors
Atropos	ANTs	Effective and versatile, provides a wide array of options to fine-tune

algorithm is trained to predict the velocity field associated to a diffeomorphic deformation, given two volumes. The resulting momentum can either be used directly or as a prior to initialize an optimization algorithm, thus drastically reducing the optimization time.

Even more promising, both in terms of accuracy as in computational efficiency, deep learning algorithms (LeCun et al., 2015; Akkus et al., 2017 Akkus et al., 2017) are likely to revolutionize the current paradigm for all segmentation and classification tasks and have already been implemented for simpler classification tasks like skull-stripping (Roy et al., 2018). This can be considered a multi-atlas approach, in which the algorithm is trained on a large number of annotated volumes. While the training step is computationally expensive it only has to be performed once; the effective runtime of the classification task can be drastically reduced. Recently, Wachinger et al. (2018) implemented a Deep Neural Network capable of outperforming state of the art methods for the segmentation of the human brain in one hour, whereas a single registration on the same machine took 2 hours to be performed. Employing a fully convolutional approach with the U-Net architecture Ronneberger et al. (2015) and Roy et al. (2018) brought the total segmentation time down to 20 s, while preserving the competitive performance in terms of accuracy, by integrating in the training procedure volumes labeled with Freesurfer, an atlas based tool (Fischl et al., 2002). As the segmentation speed is indeed one of the most important problems to be addressed right now in the field of MRI segmentation, we are likely going to see this architecture or a similar algorithms implemented as well for small rodents in the near future.

Increasing the segmentation speed will in turn facilitate research on large datasets in all the different fields in which small rodents brain MRI plays a role, from pathogenesis research to preclinical drug development, from basic neuroscience to the study of neurodegenerative diseases.

Contribution statement

RDF made the bibliographic search and drafted the paper. FG ideated and coordinated the research and revised the paper. Both authors approved the final version.

Acknowledgements

Partially supported by the Italian Ministry of Health (Ricerca Corrente). This project has received funding from the European Union's Horizon 2020 research and innovation programme under the Marie Skłodowska-Curie grant agreement No 691110 (MICROBRADAM). The content is solely the responsibility of the authors and does not necessarily represent the official views of the funding bodies.

References

Aggarwal, M., Zhang, J., Miller, M.I., Sidman, R.L., Mori, S., 2009. Magnetic resonance imaging and micro-computed tomography combined atlas of developing and adult mouse brains for stereotaxic surgery. Neuroscience 162, 1339–1350.
Akkus, Z., Galimzianova, A., Hoogi, A., Rubin, D.L., Erickson, B.J., 2017. Deep learning for brain MRI segmentation: state of the art and future directions. J. Digit. Imaging 30, 449–459.
Ali, A.A., Dale, A.M., Badea, A., Johnson, G.A., 2005. Automated segmentation of neuroanatomical structures in multispectral MR microscopy of the mouse brain. Neuroimage 27, 425–435.
Ashburner, J., Friston, K.J., 2000. Voxel-based morphometry-the methods. Neuroimage 11, 805–821.
Ashburner, J., Friston, K.J., 2005. Unified segmentation. Neuroimage 26, 839–851.
Ashburner, J., Friston, K.J., 2011. Diffeomorphic registration using geodesic shooting and gauss-newton optimisation. NeuroImage 55, 954–967.
Ashburner, J., 2007. A fast diffeomorphic image registration algorithm. Neuroimage 38, 95–113.
Avants, B.B., Epstein, C.L., Grossman, M., Gee, J.C., 2008. Symmetric diffeomorphic image registration with cross-correlation: evaluating automated labeling of elderly and neurodegenerative brain. Med. Image Anal. 12, 26–41.
Avants, B.B., Tustison, N., Song, G., 2009. Advanced normalization tools (ANTS). Insight J. 2, 1–35.
Avants, B.B., Yushkevich, P., Pluta, J., Minkoff, D., Korczykowski, M., Detre, J., Gee, J.C., 2010. The optimal template effect in hippocampus studies of diseased populations. Neuroimage 49, 2457–2466.
Avants, B.B., Tustison, N.J., Wu, J., Cook, P.A., Gee, J.C., 2011. An open source multivariate framework for n-tissue segmentation with evaluation on public data. Neuroinformatics 9, 381–400.
Bae, M.H., Pan, R., Wu, T., Badea, A., 2009. Automated segmentation of mouse brain images using extended MRF. Neuroimage 46, 717–725.
Bai, J., Trinh, T.L.H., Chuang, K.-H., Qiu, A., 2012. Atlas-based automatic mouse brain image segmentation revisited: model complexity vs. image registration. Magn. Resonance Imaging 30, 789–798.
Beg, M.F., Miller, M.I., Trouvé, A., Younes, L., 2005. Computing large deformation metric mappings via geodesic flows of diffeomorphisms. Int. J. Comput. Vision 61, 139–157.
Cardoso, M.J., Modat, M., Ourselin, S., Keihaninejad, S., Cash, D., 2012. Multi-STEPS: multi-label similarity and truth estimation for propagated segmentations. 2012 IEEE Workshop on Mathematical Methods in Biomedical Image Analysis (MMBIA) IEEE 153–158.
Cardoso, M.J., Leung, K., Modat, M., Keihaninejad, S., Cash, D., Barnes, J., Fox, N.C., Ourselin, S., Initiative, A.D.N., et al., 2013. Steps: Similarity and truth estimation for propagated segmentations and its application to hippocampal segmentation and brain parcelation. Med. Image Anal. 17, 671–684.
Chou, N., Wu, J., Bingren, J.B., Qiu, A., Chuang, K.-H., 2011. Robust automatic rodent brain extraction using 3-D pulse-coupled neural networks (PCNN). IEEE Trans. Image Process. 20, 2554–2564.
Chuang, N., Mori, S., Yamamoto, A., Jiang, H., Ye, X., Xu, X., Richards, L.J., Nathans, J., Miller, M.I., Toga, A.W., et al., 2011. An MRI-based atlas and database of the developing mouse brain. Neuroimage 54, 80–89.
Clarke, L., Velthuizen, R., Phuphanich, S., Schellenberg, J., Arrington, J., Silbiger, M., 1993. MRI: stability of three supervised segmentation techniques. Magn. Resonance Imaging 11, 95–106.
Collins, D., Neelin, P., Peters, T., Evans, A., 1994. Automatic 3D intersubject registration of MR volumetric data in standardized talairach space. J. Comput. Assist. Tomogr. 18 (2), 192–205 1994.
Cox, R.W., 1996. AFNI: software for analysis and visualization of functional magnetic resonance neuroimages. Comput. Biomed. Res. Int. J. 29, 162–173.
Dalca, A.V., Balakrishnan, G., Guttag, J., Sabuncu, M.R., 2018. Unsupervised Learning for Fast Probabilistic Diffeomorphic Registration. arXiv preprint arXiv:1805.04605.
Delora, A., Gonzales, A., Medina, C.S., Mitchell, A., Mohed, A.F., Jacobs, R.E., Bearer, E.L., 2016. A simple rapid process for semi-automated brain extraction from magnetic resonance images of the whole mouse head. J. Neurosci. Methods 257, 185–193.
Dice, L.R., 1945. Measures of the amount of ecologic association between species. Ecology 26, 297–302.
Dorr, A., Lerch, J.P., Spring, S., Kabani, N., Henkelman, R.M., 2008. High resolution three-dimensional brain atlas using an average magnetic resonance image of 40 adult C57Bl/6J mice. Neuroimage 42, 60–69.
Fischl, B., Salat, D.H., Busa, E., Albert, M., Dieterich, M., Haselgrove, C., Van Der Kouwe, A., Killiany, R., Kennedy, D., Klaveness, S., et al., 2002. Whole brain segmentation: automated labeling of neuroanatomical structures in the human brain. Neuron 33, 341–355.
Fu, Z., Lin, L., Jin, C., 2016. Symmetric image normalization for mouse brain magnetic resonance microscopy. International Conference on Advances in Mechanical Engineering and Industrial Informatics. Zheng Zhou, China.
Fu, Z., Lin, L., Tian, M., Wang, J., Zhang, B., Chu, P., Li, S., Pathan, M.M., Deng, Y., Wu, S., 2017. Evaluation of five diffeomorphic image registration algorithms for mouse brain magnetic resonance microscopy. J. Microsc. 268, 141–154.
Gutierrez-Becker, B., Mateus, D., Peter, L., Navab, N., 2017. Guiding multimodal registration with learned optimization updates. Med. Image Anal. 41, 2–17.
Harsan, L.-A., Paul, D., Schnell, S., Kreher, B.W., Hennig, J., Staiger, J.F., Von Elverfeldt, D., 2010. In vivo diffusion tensor magnetic resonance imaging and fiber tracking of the mouse brain. NMR Biomed. 23, 884–896.
Hawrylycz, M., Baldock, R.A., Burger, A., Hashikawa, T., Johnson, G.A., Martone, M., Ng, L., Lau, C., Larsen, S.D., Nissanov, J., et al., 2011. Digital atlasing and standardization in the mouse brain. PLoS Comput. Biol. 7, e1001065.
Hjornevik, T., Leergaard, T.B., Darine, D., Moldestad, O., Dale, A.M., Willoch, F., Bjaalie, J.G., 2007. Three-dimensional atlas system for mouse and rat brain imaging data. Front. Neuroinform. 1, 4.
Iglesias, J.E., Sabuncu, M.R., 2015. Multi-atlas segmentation of biomedical images: a survey. Med. Image Anal. 24, 205–219.
Jaccard, P., 1912. The distribution of the flora in the alpine zone. 1. New Phytologist 11, 37–50.
Jenkinson, M., Smith, S., 2001. A global optimisation method for robust affine registration of brain images. Med. Image Anal. 5, 143–156.
Johnson, G.A., Badea, A., Brandenburg, J., Cofer, G., Fubara, B., Liu, S., Nissanov, J., 2010. Waxholm space: an image-based reference for coordinating mouse brain research. Neuroimage 53, 365–372.
Johnson, G.A., Calabrese, E., Badea, A., Paxinos, G., Watson, C., 2012. A multidimensional magnetic resonance histology atlas of the wistar rat brain. Neuroimage 62, 1848–1856.
Jonckers, E., Van Audekerke, J., De Visscher, G., Van der Linden, A., Verhoye, M., 2011. Functional connectivity fMRI of the rodent brain: comparison of functional connectivity networks in rat and mouse. PLoS ONE 6, e18876.
Jonckers, E., Shah, D., Hamaide, J., Verhoye, M., Van der Linden, A., 2015. The power of using functional fMRI on small rodents to study brain pharmacology and disease. Front. Pharmacol. 6, 231.
Kjonigsen, L.J., Lillehaug, S., Bjaalie, J.G., Witter, M.P., Leergaard, T.B., 2015. Waxholm space atlas of the rat brain hippocampal region: three-dimensional delineations based on magnetic resonance and diffusion tensor imaging. Neuroimage 108, 441–449.

Klein, A., Andersson, J., Ardekani, B.A., Ashburner, J., Avants, B., Chiang, M.-C., Christensen, G.E., Collins, D.L., Gee, J., Hellier, P., et al., 2009. Evaluation of 14 nonlinear deformation algorithms applied to human brain MRI registration. Neuroimage 46, 786–802.
Klein, S., Staring, M., Murphy, K., Viergever, M.A., Pluim, J.P., 2010. Elastix: a toolbox for intensity-based medical image registration. IEEE Trans. Med. Imaging 29, 196–205.
Kochunov, P., Lancaster, J.L., Thompson, P., Woods, R., Mazziotta, J., Hardies, J., Fox, P., 2001. Regional spatial normalization: toward an optimal target. J. Comput. Assist. Tomogr. 25, 805–816.
Kovačević, N., Henderson, J., Chan, E., Lifshitz, N., Bishop, J., Evans, A., Henkelman, R., Chen, X., 2004. A three-dimensional MRI atlas of the mouse brain with estimates of the average and variability. Cereb. Cortex 15, 639–645.
Lancelot, S., Roche, R., Slimen, A., Bouillot, C., Levigoureux, E., Langlois, J.-B., Zimmer, L., Costes, N., 2014. A multi-atlas based method for automated anatomical rat brain MRI segmentation and extraction of PET activity. PLOS ONE 9, e109113.
LeCun, Y., Bengio, Y., Hinton, G., 2015. Deep learning. Nature 521, 436.
Lee, J., Lyu, I., Styner, M., 2014. Multi-atlas segmentation with particle-based group-wise image registration. Medical Imaging 2014: Image Processing, vol. 9034. International Society for Optics and Photonics, pp. 903447.
Leung, K.K., Barnes, J., Modat, M., Ridgway, G.R., Bartlett, J.W., Fox, N.C., Ourselin, S., Initiative, A.D.N., et al., 2011. Brain maps: an automated, accurate and robust brain extraction technique using a template library. Neuroimage 55, 1091–1108.
Li, Q., Cheung, C., Wei, R., Hui, E.S., Feldon, J., Meyer, U., Chung, S., Chua, S.E., Sham, P.C., Wu, E.X., et al., 2009. Prenatal immune challenge is an environmental risk factor for brain and behavior change relevant to schizophrenia: evidence from MRI in a mouse model. PLoS ONE 4, e6354.
Li, J., Liu, X., Zhuo, J., Gullapalli, R.P., Zara, J.M., 2013. An automatic rat brain extraction method based on a deformable surface model. J. Neurosci. Methods 218, 72–82.
Li, S.Z., 1994. Markov random field models in computer vision. European conference on computer vision Springer 361–370.
Liang, S., Wu, S., Huang, Q., Duan, S., Liu, H., Li, Y., Zhao, S., Nie, B., Shan, B., 2017. Rat brain digital stereotaxic white matter atlas with fine tract delineation in paxinos space and its automated applications in DTI data analysis. Magn. Resonance Imaging 43, 122–128.
Ma, Y., Hof, P., Grant, S., Blackband, S., Bennett, R., Slatest, L., McGuigan, M., Benveniste, H., 2005. A three-dimensional digital atlas database of the adult C57BL/6J mouse brain by magnetic resonance microscopy. Neuroscience 135, 1203–1215.
Ma, D., Cardoso, M., Modat, M., Powell, N., Holmes, H., Lythgoe, M., Ourselin, S., 2012. Multi atlas segmentation applied to in vivo mouse brain MRI. MICCAI 2012 Workshop on Multi-Atlas Labeling.
Ma, D., Cardoso, M.J., Modat, M., Powell, N., Wells, J., Holmes, H., Wiseman, F., Tybulewicz, V., Fisher, E., Lythgoe, M.F., et al., 2014. Automatic structural parcellation of mouse brain MRI using multi-atlas label fusion. PLOS ONE 9, e86576.
McIntosh, A.L., Gormley, S., Tozzi, L., Frodl, T., Harkin, A., 2017. Recent advances in translational magnetic resonance imaging in animal models of stress and depression. Front. Cell. Neurosci. 11, 150.
Murugavel, M., Sullivan Jr., J.M., 2009. Automatic cropping of MRI rat brain volumes using pulse coupled neural networks. Neuroimage 45, 845–854.
Nie, J., Shen, D., 2013. Automated segmentation of mouse brain images using multi-atlas multi-ROI deformation and label fusion. Neuroinformatics 11, 35–45.
Nie, B., Liu, H., Chen, K., Jiang, X., Shan, B., 2014. A statistical parametric mapping toolbox used for voxel-wise analysis of FDG-PET images of rat brain. PLoS ONE 9, e108295.
Oguz, I., Zhang, H., Rumple, A., Sonka, M., 2014. RATS: rapid automatic tissue segmentation in rodent brain MRI. J. Neurosci. Methods 221, 175–182.
Pagani, M., Damiano, M., Galbusera, A., Tsaftaris, S.A., Gozzi, A., 2016. Semi-automated registration-based anatomical labelling, voxel based morphometry and cortical thickness mapping of the mouse brain. J. Neurosci. Methods 267, 62–73.
Papp, E.A., Leergaard, T.B., Calabrese, E., Johnson, G.A., Bjaalie, J.G., 2014. Waxholm space atlas of the sprague dawley rat brain. Neuroimage 97, 374–386.
Patenaude, B., Smith, S.M., Kennedy, D.N., Jenkinson, M., 2011. A bayesian model of shape and appearance for subcortical brain segmentation. Neuroimage 56, 907–922.
Paxinos, G., Franklin, K.B., 2004. The Mouse Brain in Stereotaxic Coordinates. Gulf Professional Publishing.
Paxinos, G., Watson, C., 1986. The Rat Brain in Stereotaxic Coordinates/George Paxinos, Charles Watson, 2nd ed. Academic Press Sydney.
Penny, W.D., Friston, K.J., Ashburner, J.T., Kiebel, S.J., Nichols, T.E., 2011. Statistical Parametric Mapping: The Analysis of Functional Brain Images. Elsevier.
Ronneberger, O., Fischer, P., Brox, T., 2015. U-net: convolutional networks for biomedical image segmentation. International Conference on Medical Image Computing and Computer-Assisted Intervention Springer 234–241.
Roy, A.G., Conjeti, S., Navab, N., Wachinger, C., 2018a. Quicknat: Segmenting MRI Neuroanatomy in 20 Seconds. arXiv preprint arXiv:1801.04161.
Roy, S., Knutsen, A., Korotcov, A., Bosomtwi, A., Dardzinski, B., Butman, J.A., Pham, D.L., 2018b. A deep learning framework for brain extraction in humans and animals with traumatic brain injury. 2018 IEEE 15th International Symposium on Biomedical Imaging (ISBI 2018) IEEE 687–691.
Rumple, A., McMurray, M., Johns, J., Lauder, J., Makam, P., Radcliffe, M., Oguz, I., 2013. 3-dimensional diffusion tensor imaging (DTI) atlas of the rat brain. PLoS ONE 8, e67334.
Sawiak, S., Wood, N., Williams, G., Morton, A., Carpenter, T., 2009. Spmmouse: a new toolbox for SPM in the animal brain. In: ISMRM 17th Scientific Meeting & Exhibition. April. pp. 18–24.
Sawiak, S.J., Wood, N.I., Williams, G.B., Morton, A.J., Carpenter, T.A., 2013. Voxel-based morphometry with templates and validation in a mouse model of huntington's disease. Magn. Resonance Imaging 31, 1522–1531.
Schellenberg, J.D., Naylor, W.C., Clarke, L.P., 1990. Application of artificial neural networks for tissue classification from multispectral magnetic resonance images of the head. Proceedings of Third Annual IEEE Symposium on Computer-Based Medical Systems, 1990 IEEE 350–357.
Schwarz, A.J., Danckaert, A., Reese, T., Gozzi, A., Paxinos, G., Watson, C., Merlo-Pich, E.V., Bifone, A., 2006. A stereotaxic MRI template set for the rat brain with tissue class distribution maps and co-registered anatomical atlas: application to pharmacological MRI. Neuroimage 32, 538–550.
Schweinhardt, P., Fransson, P., Olson, L., Spenger, C., Andersson, J.L., 2003. A template for spatial normalisation of MR images of the rat brain. J. Neurosci. Methods 129, 105–113.
Sled, J.G., Zijdenbos, A.P., Evans, A.C., 1998. A nonparametric method for automatic correction of intensity nonuniformity in MRI data. IEEE Trans. Med. Imaging 17, 87–97.
Smith, S.M., 2002. Fast robust automated brain extraction. Hum. Brain Mapp. 17, 143–155.
Soria, G., Aguilar, E., Tudela, R., Mullol, J., Planas, A.M., Marin, C., 2011. In vivo magnetic resonance imaging characterization of bilateral structural changes in experimental parkinson's disease: a T2 relaxometry study combined with longitudinal diffusion tensor imaging and manganese-enhanced magnetic resonance imaging in the 6-hydroxydopamine rat model. Eur. J. Neurosci. 33, 1551–1560.
Thirion, J.-P., 1998. Image matching as a diffusion process: an analogy with Maxwell's demons. Med. Image Anal. 2, 243–260.
Tohka, J., Dinov, I.D., Shattuck, D.W., Toga, A.W., 2010. Brain MRI tissue classification based on local Markov random fields. Magn. Resonance Imaging 28, 557–573.
Tustison, N.J., Avants, B.B., Cook, P.A., Song, G., Das, S., van Strien, N., Stone, J.R., Gee, J.C., 2013. The ANTs cortical thickness processing pipeline. Medical Imaging 2013: Biomedical Applications in Molecular, Structural, and Functional Imaging, vol. 8672. International Society for Optics and Photonics, pp. 86720K.
Uberti, M.G., Boska, M.D., Liu, Y., 2009. A semi-automatic image segmentation method for extraction of brain volume from in vivo mouse head magnetic resonance imaging using constraint level sets. J. Neurosci. Methods 179, 338–344.
Valdes Hernandez, P.A., Sumiyoshi, A., Nonaka, H., Haga, R., Aubert Vasquez, E., Ogawa, T., Iturria Medina, Y., Riera, J.J., Kawashima, R., 2011. An in vivo MRI template set for morphometry, tissue segmentation, and fMRI localization in rats. Front. Neuroinform. 5, 26.
Veraart, J., Leergaard, T.B., Antonsen, B.T., Van Hecke, W., Blockx, I., Jeurissen, B., Jiang, Y., Van der Linden, A., Johnson, G.A., Verhoye, M., et al., 2011. Population-averaged diffusion tensor imaging atlas of the sprague dawley rat brain. Neuroimage 58, 975–983.
Wachinger, C., Reuter, M., Klein, T., 2018. Deepnat: deep convolutional neural network for segmenting neuroanatomy. NeuroImage 170, 434–445.
Warfield, S.K., Zou, K.H., Wells, W.M., 2004. Simultaneous truth and performance level estimation (STAPLE): an algorithm for the validation of image segmentation. IEEE Trans. Med. Imaging 23, 903–921.
Wood, T.C., Lythgoe, D.J., Williams, S.C., 2013. rBET: making BET work for rodent brains. Proc. Intl. Soc. Mag. Reson. Med. 21, 2706.
Xie, L., Qi, Y., Subashi, E., Liao, G., Miller-DeGraff, L., Jetten, A.M., Johnson, G.A., 2015. 4D MRI of polycystic kidneys from rapamycin-treated Glis3-deficient mice. NMR Biomed. 28, 546–554.
Yang, X., Kwitt, R., Styner, M., Niethammer, M., 2017. Quicksilver: fast predictive image registration-a deep learning approach. NeuroImage 158, 378–396.
Zhan, K., Shi, J., Wang, H., Xie, Y., Li, Q., 2017. Computational mechanisms of pulse-coupled neural networks: a comprehensive review. Arch. Comput. Methods Eng. 24, 573–588.
Zhang, Y., Brady, M., Smith, S., 2001. Segmentation of brain MR images through a hidden markov random field model and the expectation-maximization algorithm. IEEE Trans. Med. Imaging 20, 45–57.
Zhang, J., Aggarwal, M., Mori, S., 2012. Structural insights into the rodent CNS via diffusion tensor imaging. Trends Neurosci. 35, 412–421.